Polymer 50 (2009) 4028–4038

Contents lists available at ScienceDirect

Polymer

journal homepage: www.elsevier.com/locate/polymer

Evolution of EPDM networks aged by gamma irradiation – Consequences on the mechanical properties

Emilie Planes [a,b], Laurent Chazeau [a,*], Gérard Vigier [a], Jérôme Fournier [b]

[a] Université de Lyon, INSA-Lyon, MATEIS, UMR CNRS 5510, 7, avenue Jean Capelle, 69621 Villeurbanne, France
[b] NEXANS Research Center, 170 Avenue Jean Jaurès, F-69353 Lyon Cedex 07, France

ARTICLE INFO

Article history:
Received 4 March 2009
Received in revised form
15 June 2009
Accepted 15 June 2009
Available online 23 June 2009

Keywords:
Rubber
Irradiation
Mechanical properties

ABSTRACT

Different Ethylene–Propylene Diene Monomer (EPDM) elastomers with different crosslink densities have been processed in order to evaluate the influence of gamma irradiation on their properties. In the case of a major phenomenon of chain scissions, the consequences are a decrease in the modulus and also a decrease in the strain at break. This decrease in the strain at break is opposite to what is expected for materials with increasing average chain length between crosslinks. To gain more insight into the network architecture, which is presumed to be responsible for this behavior, Charlesby's approach is applied. In tandem, a computational model of the degradation is developed for improved prediction of the evolution of the elastic modulus. Using these calculations, a novel interpretation of the ultimate properties of the elastomer as a function of its architecture is proposed.

1. Introduction

Polymer materials in cables and accessories for nuclear engineering applications must typically be designed to withstand extreme environmental conditions. EPDM is one of the most common polymers for this type of application, used for instance in nuclear power plants. In this kind of application, polymer sheathing may be exposed to elevated temperatures and gamma irradiation which will accelerate its ageing and consequently degrade its useful application lifetime. The study of ageing effects due to gamma irradiation of EPDM elastomers under oxygen atmosphere has led to propose a mechanism of radio-oxidation [1,2]. This mechanism artificially induces an accelerated evolution of the mechanical properties of material. Indeed, chain scissions occur, counterbalanced by a crosslinking mechanism which depends on the initial crosslinking of the material, which, in turn, leads to the modifications of the macroscopic mechanical properties [3–7]. The consequence of such ageing, at temperatures higher than the melting temperature of the EPDM crystallites, is a decrease in the material stiffness. Moreover, the presence of crystallites at ambient temperature attenuates this effect [8,9].

Although a qualitative relationship between the macroscopic mechanical properties of the aged samples and the degradation time can easily be proposed, a true understanding of the consequences of degradation of elastomer network structure on its mechanical behavior is much more difficult. This difficulty comes from the fact that there remain several unanswered questions concerning the mechanical behavior of such materials. In particular, the role of network heterogeneities, such as that of crosslink density or the presence of free chains and dangling chains, is still under debate [10–13]. The role of the network imperfections is clearly evident in results from previous modeling efforts presented in the literature to date. One can cite the early work of Termonia [14,15], who studied the network connectivity and its mechanical properties, or the work of Grest et al. [16], where particular attention was paid to the influence of strand length, dangling ends and loops. Some experimental studies also infer that network imperfections such as free chains reduce the tensile strength and simply result in a "diluted" network [10]. Moreover, the pioneering work of Mark and his collaborators on the effect of the elastomer network architecture stresses the importance of the distribution of chain lengths between crosslinks in the strength properties of elastomer [11–13].

Complementing previous experimental study of model elastomers, elastomer degradation by irradiation can provide additional experimental insights into the nature of underlying relationships between network microstructure and mechanical properties (elastic modulus, ultimate properties), since irradiation enables a controlled, progressive manipulation of this microstructure as a function of irradiation dose. Such an approach nonetheless requires a proper understanding of the microstructural evolution of the materials during ageing. Some information on this evolution

* Corresponding author. Tel.: +33 47 243 6130; fax: +33 47 243 8528.
E-mail address: laurent.chazeau@insa-lyon.fr (L. Chazeau).

0032-3861/$ – see front matter © 2009 Elsevier Ltd. All rights reserved.
doi:10.1016/j.polymer.2009.06.036

can be obtained by using Charlesby's approach [17,18]. Indeed, this enables to relate crosslinking and scission kinetic to the evolution of the sol fraction. However, the statistical principles behind Charlesby's approach prohibit explicit quantification of network imperfections. The only way to obtain such quantification is to model the network architecture and extract the pertinent parameters describing its real-world behavior. Recent efforts have therefore been increasingly devoted to modeling the molecular dynamics of the formation of polymer networks via the crosslinking process. Among them, one can cite the recent work of Rottach [19–21] who extended his research to the crosslinking process of network during stretching. Though of obvious interest, this type of model is difficult to directly apply to the case of any particular experimental study. In the specific case of irradiation, it can in fact be more revealing to use a simpler description of the network architecture based on experimental data, in order to expose the direct relationship between mechanical properties of materials and their exposure to radiation.

Thus, in this work, different EPDM networks are elaborated: pure gum (non-crosslinked EPDM) and EPDM crosslinked by peroxide, both aged by gamma irradiation at room temperature under oxygen atmosphere, and EPDM crosslinked by peroxide at various degrees. Note that, given the semi-crystalline nature of the EPDM at room temperature [9], the work described in the article concerns EPDM at 80 °C, i.e. above its melting temperature. The materials are tested by mechanical test, swelling behavior and thermoporosimetry. In addition, a modeling of the network architecture is presented, which enables a description of evolution in relation with the experimental data. Our results lead us to conclude that irradiation causes significant defects in the network structure. The level of defects is in fact so high in rubber materials that their mechanical properties can in fact no longer be correlated at all with the standard measures of crosslink density or length of chain between crosslinks.

2. Experimental

2.1. Materials

The EPDM elastomer (Nordel IP NDR 3722 P from Dow Chemical Company) is composed of 70% ethylene, 29.5% propylene and 0.5% ENB. An analysis by gel permeation chromatography (GPC) gives the following results:

$$\overline{M}_w = 39,300\ \mathrm{g/mol}, \quad \overline{M}_n = 5140\ \mathrm{g/mol}$$

EPDM plates (1 mm) are produced with two formulations: pure gum (E-NC) and crosslinked elastomer (E-CR).

The samples are processed following three steps. The first step involves mixing the matrix and introducing a crosslinking agent to the polymer. Specifically, after 5 min of mixing in an internal mixer, peroxide is added. Its dispersion is permitted for 10 min at low temperature (80 °C) to prevent any reaction of the crosslinking system. In order to obtain a better dispersion, the second step is mixing in an external mixer (cylinders) for 10 min at low temperature (80 °C). During the last step, the compound is pressed over a 10-min period into 1-mm-thick films at 170 °C, in order to promote a crosslinking reaction. The crosslinking agent we used is the dicumyl peroxide (Perkadox BC-FF from Akzo Nobel), introduced at 3 phr. The curing time (t_{98} at 170 °C) is determined from torque measurements performed with a MOSANTO analyzer. During curing of ethylene–propylene elastomer [22,23], the peroxide decomposes into radicals at elevated temperature, which results in the formation of peroxy radicals. They can react with the polymer chains by abstraction of hydrogen atoms to produce macroradicals. Two types of chemical crosslinks are formed, one type via combination of peroxide-induced EPDM macroradicals and the other one via addition of the macroradicals to the residual double bonds of the termonomer. Actually, peroxide cure of EPM (without termonomer) is relatively inefficient. This is mainly due to the scission reactions occurring on tertiary radicals created by H-abstraction in the propylene sequence. Moreover a total efficiency of peroxide is usually inhibited by the occurrence of all kinds of auxiliary reactions, such as alternative peroxide decomposition pathways leading to inert products, combination of peroxide-derived radicals and/or disproportionation of radicals.

Two elastomers with smaller crosslinking degrees are produced as a final result, by choosing different curing times: 2 min, 3 min. They will be called E-CR2 min and E-CR3 min (see Table 1). As the soluble fraction in all crosslinked samples is zero, we can assume that all chains are crosslinked. The samples are then artificially exposed to gamma radiation as described below.

2.2. Ageing conditions

E-NC and E-CR are exposed to gamma radiation of a ^{60}CO source at a dose rate of 1 kGy/h at room temperature in an oxygen atmosphere for doses 50, 165, 300, 510 kGy (Arc Nucleart – Grenoble France). The samples are stored under vacuum at room temperature.

Radio-oxidation of EPDM macromolecules leads to the observation by IR spectroscopy of an increase in absorbance in the hydroxyl absorption region (3800–3000 cm^{-1}) [1,2] corresponding to the formation of alcohols, acids and hydroperoxides. The formation of carbonyls can also be evidenced by the absorption maximum at 1713 cm^{-1} with several shoulders around 1785, 1755, 1740, and 1695 cm^{-1} [1]. Analysis of the oxidation product distributions within the oxidized E-CR is made for E-CR-510, and the variations in absorbance at 1713 cm^{-1} are chosen to characterize the product distributions according to the thickness. The oxidation profile is found flat for this dose, which indicates that, in these conditions of irradiation, the oxidation processes are homogeneously distributed within the sample. The samples will be named hereafter E-CR-XXX and E-NC-XXX with XXX denoting the radiation dose.

2.3. Instruments

2.3.1. Swelling measurements

Samples with an initial mass M_i are introduced into a xylene composition over an 8-day period to permit them to achieve swelling equilibrium. Then the materials with swelled mass M_s are dried under vacuum at 60 °C for 24 h and weighted in order to obtain their dry mass M_d. The soluble fraction F_s and the swelling ratio Q are calculated from the following relations:

$$F_s = 1 - \frac{M_d}{M_i} \tag{1}$$

Table 1
Composition and swelling data of the studied materials (the proportions are expressed in phr: per hundred parts of matrix).

	EPDM	Peroxide	Curing time (min)	F_s (%)
E-NC	100	–	–	100
E-CR	100	3	10	0
E-CR3 min	100	3	3	0
E-CR2 min	100	3	2	0

$$Q = 1 + \frac{\rho_{polymer}}{\rho_{xylene}} \frac{M_s - M_d}{M_d} \quad (2)$$

Matrix network chain density in the swollen materials can be estimated from swelling ratio in xylene Q using the Flory–Rehner equation [24]. This equation depends on the network functionality f (non-aged crosslinked samples have a functionality 4), and χ_1 the Flory–Huggins polymer–solvent dimensionless interaction term. It is noteworthy that the functionality f is decreased as a result of material ageing. More importantly, the value of the Flory–Huggins parameter is difficult to estimate, especially after material degradation, since the polarity of the chemical composition can be strongly affected. Moreover, the result calculated from the Flory–Rehner equation is strongly sensitive to this value. These two observations suggest considering with caution the crosslink density values deduced using this technique. Therefore, we will only consider the swelling ratio and the sol fraction as reliable data. We are supported in this choice by the recent paper of Valentin et al. [25] who clearly demonstrate the uncertainties in the determination of elastomer network characterized by swelling technique.

2.3.2. Tensile tests

Tensile tests are performed on an MTS device with a temperature-controlled chamber. An image processing acquisition system (Apollor VideoTraction System) is used to obtain the true stress–strain curve. Experiments are carried out at 80 °C (above the melting temperature) with a 0.01 s^{-1} true strain rate. The samples are dumbbell-shaped with typical dimensions $20 \times 4 \times 1$ mm^3. For each material, three specimens are tested. In the figures shown only one test is reported, but the average stress and strain at break of the three specimens, with error bars, are given in Fig. 8.

The elastic modulus E is calculated as the slope at the origin of the true strain–true stress curve. The shear modulus G is deduced from the tensile elastic modulus E, assuming that the material, like any rubber, is quasi-incompressible: The Poisson coefficient is therefore approximated to 0.5.

2.3.3. Thermoporosimetry

One way of quantifying the heterogeneity of an elastomer network is by observing the melting or freezing point of adsorbed solvent within the elastomer network. This technique is generally called thermoporosimetry. This experiment is based on the fact that solvent molecules constrained to small volumes form only relatively small crystallites upon crystallization and therefore exhibit lower crystallization temperatures [26]. Broad distributions of cavity sizes should give rise to broad distributions of crystallite sizes and thus crystallite melting points [27]. Therefore, differential scanning calorimetry measurements performed on swollen sample with solvent molecules constrained in the pores can give evidence of several crystallization temperatures, which are indicative of the pore sizes and of the distributions of these sizes.

The samples are therefore swollen in cyclohexane. Then they are carefully extracted and put into an aluminum crucible fully filled with the same solvent. The melting behavior of the solvent in the samples is studied using a Perkin–Elmer Pyris Diamond differential scanning calorimeter (DSC). The temperature and heat flow of the DSC are calibrated using a standard reference (Indium). A cooling scan is first run at 10 °C/min from room temperature to −50 °C and the instrument held isothermally at −50 °C for 2 min. This is followed by a heating scan at 10 °C/min up to +40 °C. While increasing temperature from −50 °C to +40 °C, a first peak appears for swollen network which corresponds to the melting of the cyclohexane entrapped in the network. Then a second strong peak corresponding to the melting point of the free cyclohexane (in excess) is visible at around 0 °C. We will return to the analysis procedure of the experimental results later in this article.

3. Results

3.1. Degradation kinetic

The evolutions of Q and of soluble fraction F_s with the irradiation dose for E-CR are shown in Fig. 1a). Between 0 and 50 kGy, we can only note a little evolution of F_s while Q remains constant. This means that chain scissions and crosslinking are in competition. After 50 kGy, chain scissions seem to be the most important phenomenon: Q rapidly increases with the irradiation dose as well the soluble fraction F_s. The evolutions of Q and F_s with the irradiation dose for E-NC are also shown in Fig. 1b. F_s decreases with irradiation dose, then stabilizes and begins to increase at 510 kGy. Q follows the same evolution. Between 0 and 300 kGy, the major phenomenon is crosslinking while at higher doses the main occurring process is chain scission. The minimum Q value ($Q = 25$) is still large compared to the initial Q value of unaged E-CR (at 0 kGy, $Q = 3.7$). This means that the crosslinking process of E-NC by irradiation is rapidly counterbalanced by chain scissions.

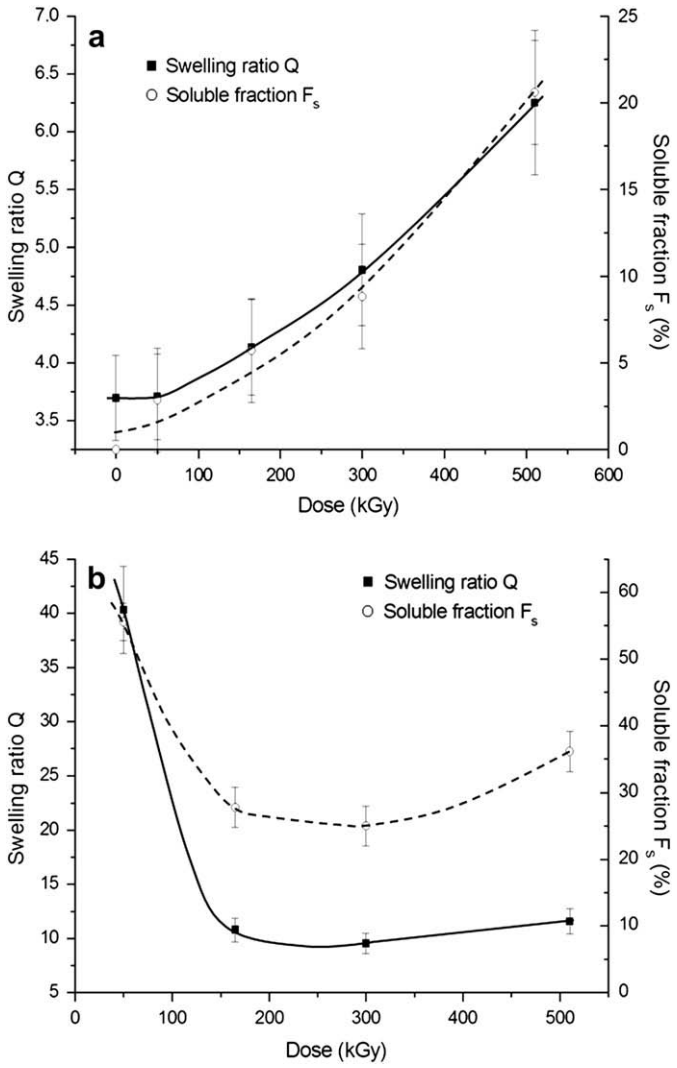

Fig. 1. Evolution of the swelling ratio Q and the soluble fraction F_s with an increasing irradiation dose for (a) E-CR and for (b) E-NC (continuous and dashed lines are guidelines).

These results are in agreement with the evolution of the experimental elasticity moduli of E-NC and E-CR as a function of the irradiation dose, which are presented in Fig. 2. The major chain scission phenomenon occurring under irradiation is evidenced for E-CR as a rapid decrease in the modulus of elasticity. The modulus slightly increases at the first dose (50 kGy), confirming the occurrence of an initial crosslinking. In the case of E-NC, first an increase in the modulus is observed, significant of a major crosslinking phenomenon. Then above 165 kGy, chain scissions mainly take place as evidenced by the modulus decrease.

Using affine network theory, the active chains concentration ν_c can be deduced from the modulus G, following the equation [24]:

$$\nu_c = \frac{G}{RT}(1 - F_s)^{-1/3} \tag{3}$$

Fig. 3 presents the evolution of deduced active chain concentration of E-CR sample. As chain scissions dominate beyond 50 kGy, and in order to estimate the chain scission kinetic action independent of the crosslinking process, we have chosen to fit the experimental ν_c data by an exponential decay law at radiation doses above 50 kGy:

$$\nu_c = \nu_0 \exp\left(\frac{-G_s}{\nu_0} D\right) \tag{4}$$

where D is the radiation dose.

Note that for small radiation doses, this law can be approximated as:

$$\nu_c = \nu_0 - G_s D \tag{5}$$

with ν_0 as the initial active chain density and G_s as the chain scission yield (mol/J) of the chains belonging to the network. The parameters deduced from the fit are: $\nu_0 = 4.15 \times 10^{-4}$ mol/cm^3 and $G_s = 8.1 \times 10^{-7}$ mol/J. Khelidj et al. [28] have estimated from their kinetic model a chain scission yield for two polyethylenes studied by Decker et al. [29] irradiated at 0.292 Gy s^{-1} (1.05 kGy h^{-1}) with different crystallinity ratios: 50% and 75%. The values are respectively 3.3×10^{-7} mol/J and 2.6×10^{-7} mol/J. They can be compared to the G_s value deduced from our fit. In our case, the chain scission yield is higher. This difference could be explained by the lower crystallinity of our samples compared to that in the previous studies. Indeed, in the crystalline regions the macromolecules have very small mobility and the oxygen is almost unable to diffuse;

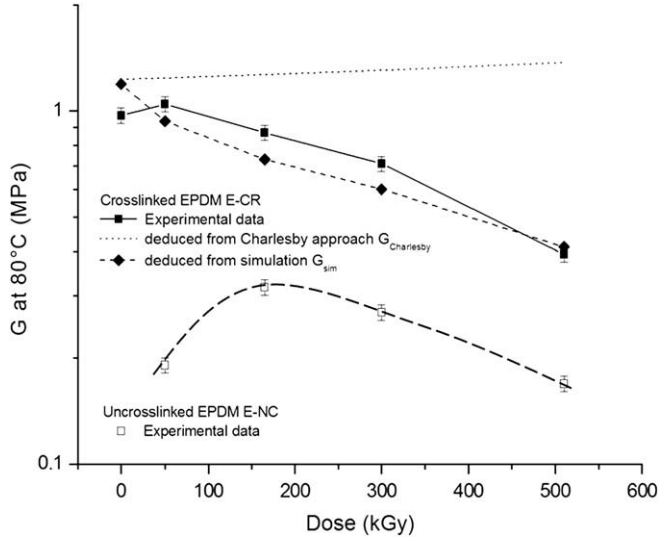

Fig. 2. Evolution of the shear modulus G at 80 °C with an increasing irradiation dose for E-NC and for E-CR.

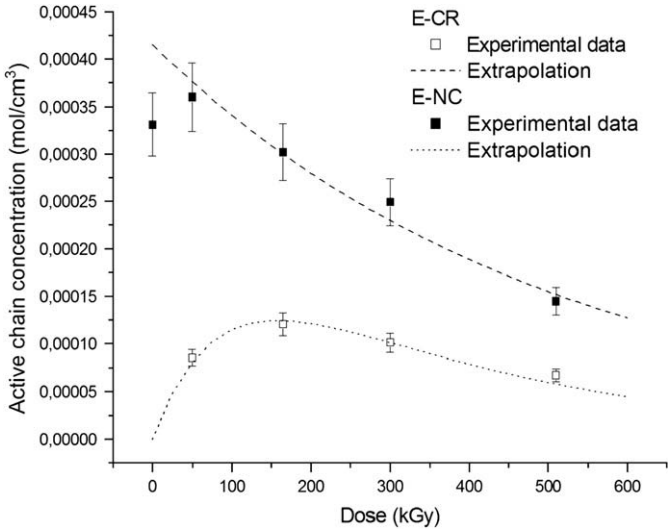

Fig. 3. Evolution of the apparent crosslink density versus irradiation dose with the phenomenological fits for E-CR and E-NC.

diffusion constants for crystalline phase are small, around 8 or 9 orders of magnitude smaller than in the amorphous region. For that reason, chain scissions mostly take place in the amorphous regions. Taking into account the crystallinity of our materials (around 11%), our chain scission yield related to the amorphous part (9.1×10^{-7} mol/J) is between the values deduced from the Decker data (6.6×10^{-7} mol/J and 10.4×10^{-7} mol/J respectively). An alternative explanation is as follows: the studied rubber is a copolymer with a non-negligible fraction of propylene and this termonomer is more sensitive to chain scissions [30]. The ν_0 value deduced from our fit can be seen as the assumed initial crosslink density value of an E-CR that would have given the experimental crosslinking density evolution as a function of the irradiation dose, if only the chain scission processes had taken place. Such value corresponds to a molar mass between crosslinks of 2200 g/mol (calculation made with an EPDM density of 0.9).

Fig. 3 also presents the apparent crosslinked density of E-NC deduced from Equation (3), as a function of the irradiation dose. In this case, the crosslinking process is significant and precludes a similar curve fit. However, the material degradation can be seen as the successive occurrence of a crosslinking process, which leads to a material with a given crosslink density, submitted afterwards to a degradation process similar to that occurring in the E-CR sample. The crosslinking process is assumed to be governed by the gap between the actual crosslink density ν'_0 and an equilibrium crosslink density ν_{0eq}. This can be empirically modeled by the formula:

$$\nu'_0 = \nu_{0eq}\left(1 - \exp\left(\frac{-2G_c}{\nu_{0eq}} D\right)\right) \tag{6}$$

with G_c as the crosslinking yield (proportion of crosslinked monomer units per energy unit). The factor of two in the exponential represents the fact that one crosslink involves two monomer units.

From this, the assumption can be made that the scission kinetic is the same as for E-CR. Under this assumption, the apparent active chain density ν_c of E-NC is:

$$\nu_c = \nu'_0 \exp\left(\frac{-G_s D}{\nu_{0eq}}\right) = \nu_{0eq}\left(1 - \exp\left(\frac{-2G_c D}{\nu_{0eq}}\right)\right)\exp\left(\frac{-G_s D}{\nu_{0eq}}\right) \tag{7}$$

The corresponding fit is very satisfactory and is presented in Fig. 3. The parameters deduced from the fit are $\nu_{0eq} = 2.7 \times 10^{-4}$ mol/cm^3, which is assumed to be constant, and $G_c = 1.15 \times 10^{-6}$ mol/J. The maximal active chain density obtained by peroxide cure, and deduced from E-CR was previously found to be 4.15×10^{-4} mol/cm^3. Both values are of the same order. Thus, within the assumption of this phenomenological model, the number of crosslinking sites potentially activated by gamma irradiation is on the same order as that generated by peroxide crosslinking. Note that this phenomenological approach implicitly makes the strong assumption that the crosslinking process involved during the degradation mechanism would lead, without the concomitant occurrence of chain scissions, to a crosslinking of the network without any sol fraction (since otherwise one must account for the possible scission of chains of the sol fraction).

To gain further insight into the kinetic degradation of the E-CR material, the Charlesby–Pinner approach is used [17]. It provides a simple expression relating sol fraction F_s to irradiation dose D, in the specific case of an initial random distribution of the molar weight of the polymer chains under the assumption that crosslinking and scission occur at random.

$$F_s + \sqrt{F_s} = \frac{p(D)}{q(D)} + \frac{1}{q(D)u_1} \tag{8}$$

where D is the irradiation dose, $q(D)$ is the proportion of crosslinked monomer units and $p(D)$ is the number of chain scissions per monomer unit. The parameter u_1 is related to the initial distribution:

$$u_1 = \overline{M}_n/w \tag{9}$$

with $\overline{M}_n$ and w as the average number molar weight and the molar mass of the polymer unit.

The relation (8) holds whether or not main-chain fracture occurs simultaneously with crosslinking. Indeed this relation allows one to consider a material undergoing simultaneous crosslinking and scission as it first experienced scission, only then followed by crosslinking. This relation is only valid in the case of an initial random distribution. For other distributions, there is no analytical expression. The relation remains valid, however, for large numbers of scissions, since the initial distribution tends to be a random after a large number of scissions.

In our study, as shown previously, the E-CR material is submitted to a competition of the phenomena of crosslinking and chain scissions between 0 and 50 kGy. After 50 kGy, the major phenomenon is scissions. Thus the proportion of crosslinked monomer $q(D)$ is taken independent on D, as a constant q_f. The value of this constant can be estimated from the elastic modulus data. The average molar mass between crosslinks of the modeled E-CR is estimated equal to 2200 g/mol through the previous extrapolation at 0 kGy of the active chain concentration (cf. Fig. 3). This is equivalent to considering an initial average chain length between crosslinks N_c of 66 units (calculation made with an EPDM unit with a molar mass of 32.6 g/mol). We can also make the assumption (as Charlesby did [17,18]) that $p(D)$ is proportional to irradiation dose.

Thus relation (8) becomes affine in D:

$$F_s + \sqrt{F_s} = \frac{p_0 D}{q_f} + \frac{1}{q_f u_1} \tag{10}$$

with p_0 as a constant. As shown in Fig. 4, the experimental evolution of $F_s + \sqrt{F_s}$ versus irradiation dose is in good agreement with the relation (10). Taking for p_0/q_f a value of 1.1×10^{-3} kGy^{-1}, a chain scission yield $G_{s\text{-Charlesby}}$ can be deduced: It is found that 5.2×10^{-7} mol/J is in good agreement with the previous value G_s

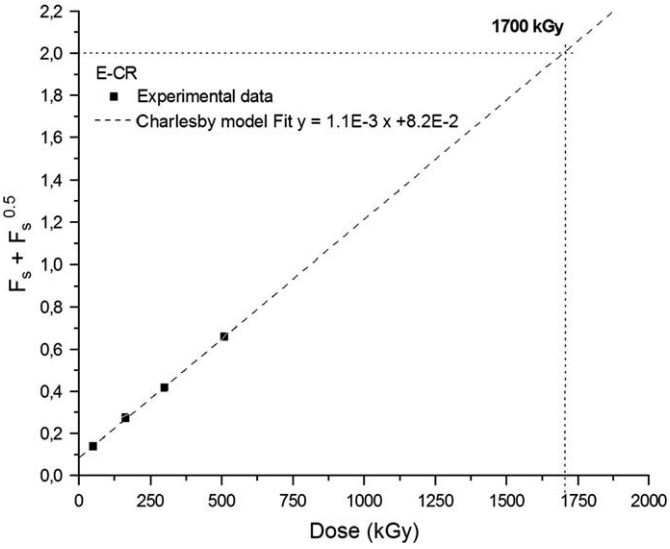

Fig. 4. Evolution of $F_s + \sqrt{F_s}$ versus irradiation dose, compared with relation (8).

(8.1×10^{-7} mol/J). This value is also in agreement with the work of Decker et al. [29] taking in account the crystallinity ratio. The number of scissions per monomer unit as a function of the irradiation dose calculated using the deduced p_0 value is presented in Fig. 5.

Returning to Fig. 4, we note that the intercept point of the affine fit is 8.2×10^{-2}. Within the assumption of an initially random distribution of the polymer, an average number molar weight of the unlinked polymer can be estimated to be approximately 26,000 g/mol. This value is larger than that of our polymer ($\overline{M}_n$ = 5140 g/mol), but this discrepancy could be explained by the fact that the initial molar weight distribution of the polymer is not random, in other words that Equation (10) is not valid for low radiation doses. From the same fit of Fig. 4, we can also calculate the irradiation dose required to reach the complete degradation of the polymer, that is, when the soluble fraction is equal to 1. The extrapolated value is 1700 kGy.

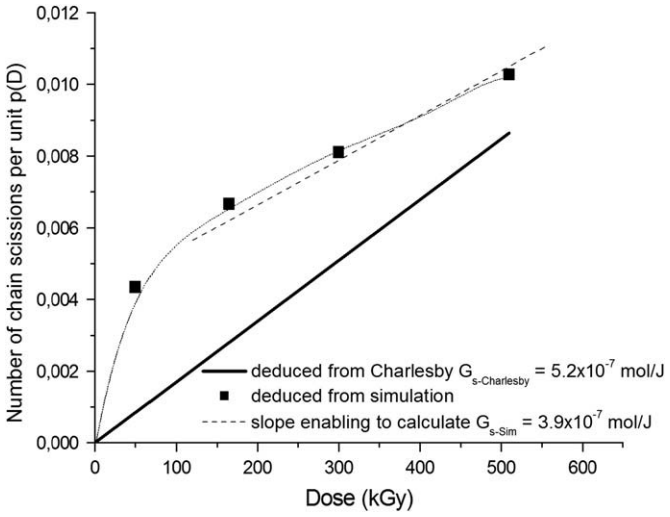

Fig. 5. Number of chain scissions as a function of the irradiation dose $p(D)$, deduced from Charlesby and from the simulation and the experimental soluble fractions for E-CR.

Charlesby [17] also proposed a relationship between the average weight between crosslinks M_c in the gel, the sol fraction and the crosslink density:

$$M_c = \frac{w}{q_f(1+F_s)} \tag{11}$$

From this relation and the work of Flory [24], it is possible to derive the shear modulus $G_{Charlesby}$ of the E-CR material:

$$G_{Charlesby} = \frac{\rho RT(1-F_s)^{1/3}}{M_c} \tag{12}$$

As shown in Fig. 2, Equation (12) does not describe properly the evolution of the shear modulus of E-CR. Therefore, while Charlesby's approach is very convincing for the description of the sol fraction evolution, its M_c calculation cannot aid in predicting the modulus. This is not unexpected since Equations (11) and (12) do not take in account the irregularities of the network provoked by the chain scission process. The sol fraction used in Equation (12) is not entirely representative of the inactive chains, because the dangling chains do not take part in the network mechanical properties (if entanglement effects are neglected). Moreover the average molar weight between active crosslinks M_c is underestimated: active chains may include inactive crosslinks, therefore their effective length should be calculated from the length between active crosslinks alone. (Note that the increase predicted by Charlesby is due to the fact that chain scissions first occur in the longest chains which automatically lead to a decrease in M_c.) An accurate prediction of the modulus must include consideration of these aspects.

3.2. Large strain behavior

Consequences of irradiation on the mechanical behavior of E-NC and E-CR at large strains are presented in Figs. 6–8 respectively. In agreement with results previously obtained with E-NC (from 0 to 165 kGy), the stress level for a given strain increases. This confirms that the predominant phenomenon taking place is in fact crosslinking. Subsequently, from 165 kGy to 510 kGy, chain scissions predominate, resulting in a decrease in the stress level. Note that the non-irradiated E-NC flows in the clamps. This was expected

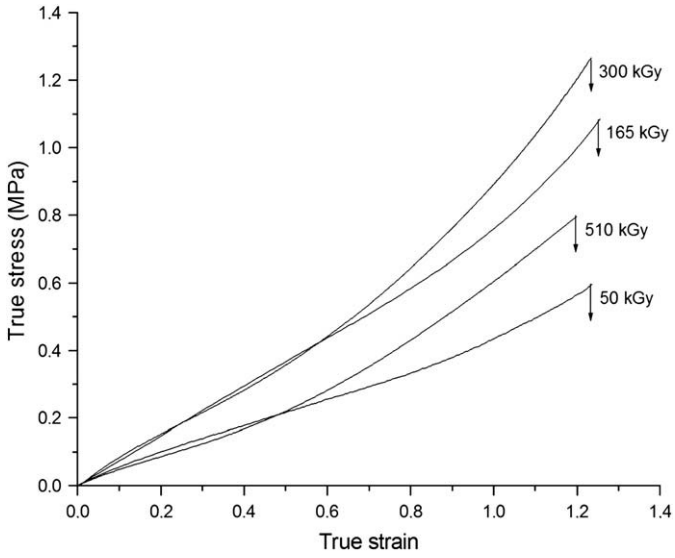

Fig. 6. Large deformation behaviors at 80 °C of E-NC.

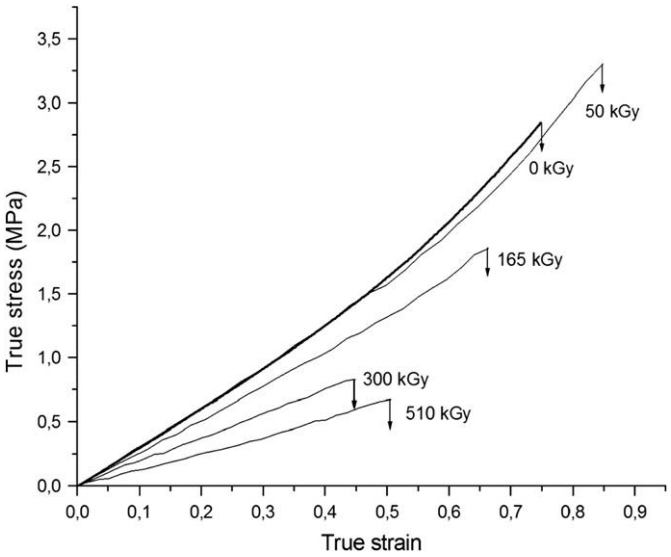

Fig. 7. Large strain behaviors at 80 °C of E-CR.

since the testing temperature is much higher than the glass transition temperature of the polymer. This indicates that the entanglements contribution to the stiffness of the irradiated materials can be neglected at 80 °C. Concerning the rupture behavior, the formation of crosslinks and chain scissions under irradiation does not significantly influence the elongation at break, though the evolution of the stress at break follows the same trend as the evolution of the elastic modulus.

Concerning E-CR samples, the evolution of the stress level at a given strain with the irradiation dose is also in agreement with the previous results. However, except with the E-CR aged at 50 kGy, ageing under irradiation leads to a decrease in the elongation at break and to the disappearance of a strain hardening phenomenon prior to rupture. In Fig. 9 we compare E-CR2 min, E-CR3 min, E-NC-165, E-CR-0, 300, and 510. As reported in Table 2, though their moduli are comparable, E-CR2 min, E-CR3 min and E-CR-300 exhibit very different rupture behaviors, the latter having much smaller stress and strain at break. E-CR-510 and E-NC-165 also have roughly the same modulus, but the true strains at break are different (with a 2.5 ratio). It seems quite reasonable to conclude that there is no direct correlation between modulus and rupture behavior. The swelling ratios of the same samples are also reported in the same table. They also demonstrate an absence of correlation between Q and the rupture behavior.

In summary, the mechanical measurements at small deformations are in agreement with the swelling measurements, but the evolution of the rupture behavior cannot be explained by a decrease in active chain concentration alone. During ageing the degradation induces defects such as dangling chains, free chains, and network heterogeneities that may in fact be primarily responsible for the rupture behavior observed. Studies of Mark et al. [11,12] suggest that a large proportion of short chains leads to a brittle behavior. This stresses the need for better characterization of network heterogeneities.

3.3. Network heterogeneity

The network heterogeneity has been characterized by thermoporosimetry. Fig. 10 presents the DSC curves of the swollen (in cyclohexane) irradiated E-CR, E-NC-165, E-CR-2 min and E-CR-3 min. The melting peaks are shifted towards higher temperatures

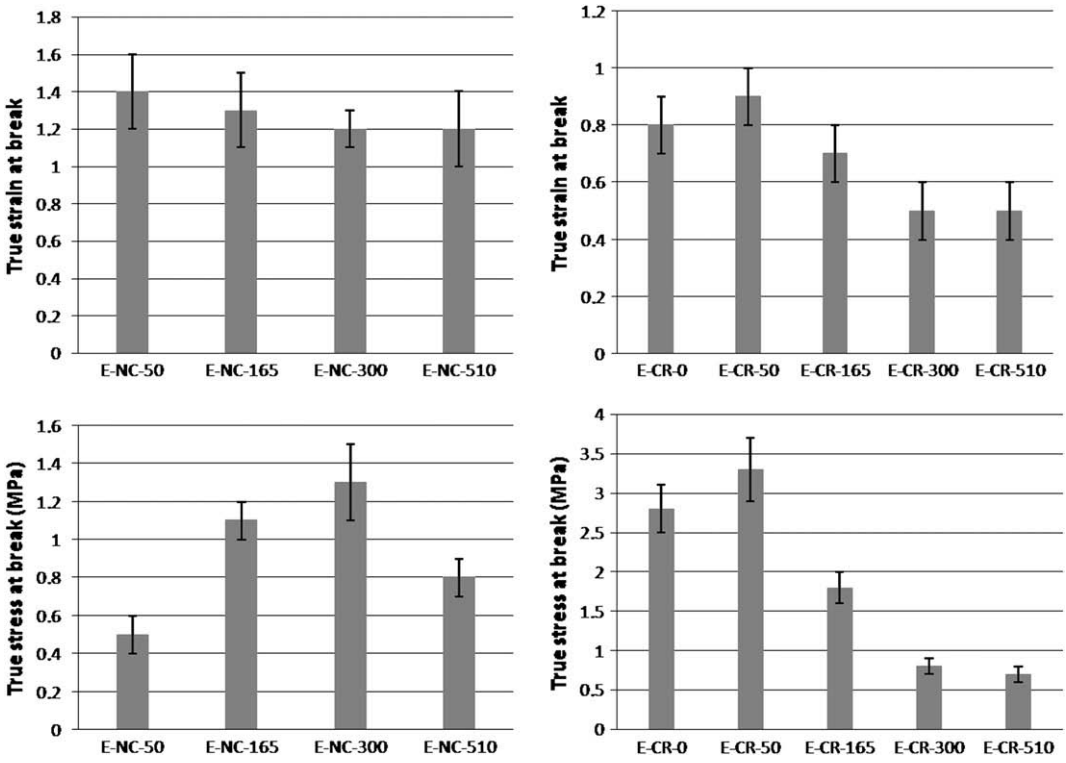

Fig. 8. Average stresses and strains at break for tensile tests at 80 °C of E-NC and of E-CR.

with increasing radiation dose, indicating that the size of solvent pockets increases. With E-NC-165, even though it has the highest modulus of the irradiated E-NC series, the melting peak overlaps the free solvent peak, meaning that the solvent pockets are very large. This is in alignment with the previous results showing that E-NC irradiated is only very slightly crosslinked. Thus for this kind of material, the distribution of pockets sizes cannot be accurately evaluated.

The distributions of pocket sizes are extracted from the following treatments. The Gibbs–Thomson equation describes the melting temperature of liquids confined into a porous medium T_m [27] as follows:

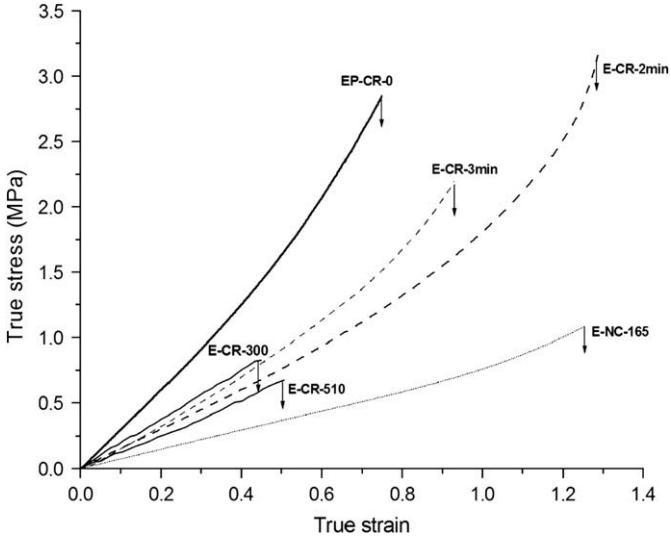

Fig. 9. Large deformation behaviors at 80 °C of irradiated elastomers and of cross-linked rubbers with different curing times.

$$T_m^0 - T_m = \frac{2\sigma_{SL}T_m^0}{L\Delta H_f} \tag{13}$$

where σ_{SL} is the solid–liquid interface energy, ΔH_f is the bulk heat fusion (6.3 J/g), L refers to the crystal size (here the solvent pocket size), and T_m^0 is the melting temperature for the bulk material (i.e. solvent), 0 °C.

The distributions can be obtained by differentiating Equation (13). As σ_{SL} is unknown, we have expressed these distributions as function of a parameter L_f. L_f is the highest pocket size measured in all the samples. This pocket size corresponds to a melting temperature T_f. M is the sample weight.

$$\frac{dM}{dL} = A\frac{\frac{dH}{dT}\left(T_m^0 - T\right)^2}{L_f} \tag{14}$$

with

$$A = \frac{1}{\Delta H_f\left(T_m^0 - T_f\right)} \tag{15}$$

Table 2
Average stresses and strains at break of materials presented in Fig. 7 compared to their soluble fraction F_s and their swelling ratio Q.

Sample name	Soluble fraction F_s (%)	Elastic modulus at 80 °C(MPA)	Swelling ratio Q	Strain at break	Stress at break (MPa)
E-CR-0	0	2.9 ± 0.3	3.7	0.8 ± 0.1	2.8 ± 0.3
E-CR-300	8.8	2.1 ± 0.2	4.8	0.5 ± 0.1	0.8 ± 0.1
E-CR-510	20.6	1.2 ± 0.1	6.2	0.5 ± 0.1	0.7 ± 0.1
E-NC-165	27.8	1.8 ± 0.2	10.8	1.3 ± 0.2	1.1 ± 0.1
E-CR-3 min	0	1.5 ± 0.2	5	0.7 ± 0.1	2.7 ± 0.4
E-CR-2 min	0	0.8 ± 0.1	5.7	1.1 ± 0.1	3.4 ± 0.5

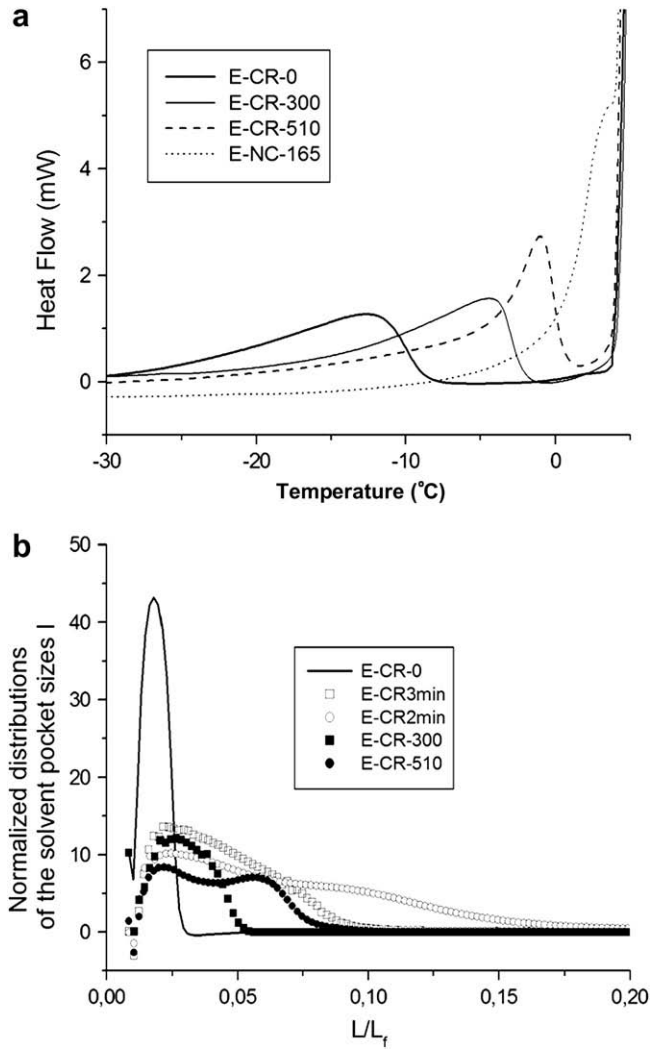

Fig. 10. (a) DSC analysis of the E-CR-0, 300, 510 and E-NC-165 swelled in cyclohexane, (b) Normalized distributions of the solvent pocket sizes *I* for different materials.

The results from the analysis are presented in Fig. 10b). The normalized distribution of the solvent pocket sizes *I* is calculated using the following relation:

$$I = \frac{1}{AM}\frac{\mathrm{d}M}{\mathrm{d}L} \tag{16}$$

The average size of the solvent pockets as well as their size distribution increases with the radiation dose. Two peaks are visible for the most irradiated material. E-CR3 min and E-CR2 min have a wide distribution of solvent pocket sizes. Thus, an increasing curing time leads to an increase in the crosslink density and a narrower distribution of the chain length in between crosslinks. E-CR2 min presents the largest distribution. E-CR3 min and E-CR-510 have comparable distributions, even though their mechanical properties are very different. Thus, sole consideration of distribution alone is insufficient to explain rupture behavior. It is noteworthy that E-CR-510 and E-CR3 min have a very different sol fraction, 20% and 0% respectively. The sol fraction can be made of short portions of chains, and also of chain agglomerates which are mechanically inactive. This might very well be the reason behind the difference in mechanical properties of those materials. In order to have more insights on this aspect, a modeling approach of the elastomer architecture is necessary.

3.4. Simulation

A model was developed to describe the degradation kinetic of the studied elastomer networks. Similarly to Termonia's work [14,15], this network can be modeled by way of nodes and links, where tetrafunctional nodes describe the elastomer crosslinks, and the links of polymer chains between those nodes. Each link is defined by its ending nodes and its length, i.e. the number of constitutive units, with a unit being assimilated into a monomer. To avoid border effects, periodicity of the network is implemented: The nodes of one edge are linked to the nodes of the opposite edge (see Fig. 11). A scission reaction corresponds to the statistically random breakage of one unit in the network, meaning that the more probable breakage of the long chains can be accounted for. (Note that the breakage is applied to the chain units and not to the nodes.) In parallel, a calculation is performed to calculate the average length of the dangling chains. This calculation keeps the memory of the length of broken chains so that they can be submitted to successive breakages. This enables the calculation of the part of the sol fraction which is due to successive breakages of a link. The second part of the sol fraction is the fraction of the isolated link agglomerates that are not linked to the polymer network. Moreover, the polymer network resulting from the degradation can be seen as a network backbone grafted by a more or less complex branched structure. This network backbone is numerically obtained by iterative elimination of all chains having a free end. This process enables the calculation of the molar mass distribution of the branches either linked or unlinked to the network. The molar mass distribution between active nodes of the chain constituting the "clean" network backbone is then deduced by considering that the chains are part of the same chain if they are

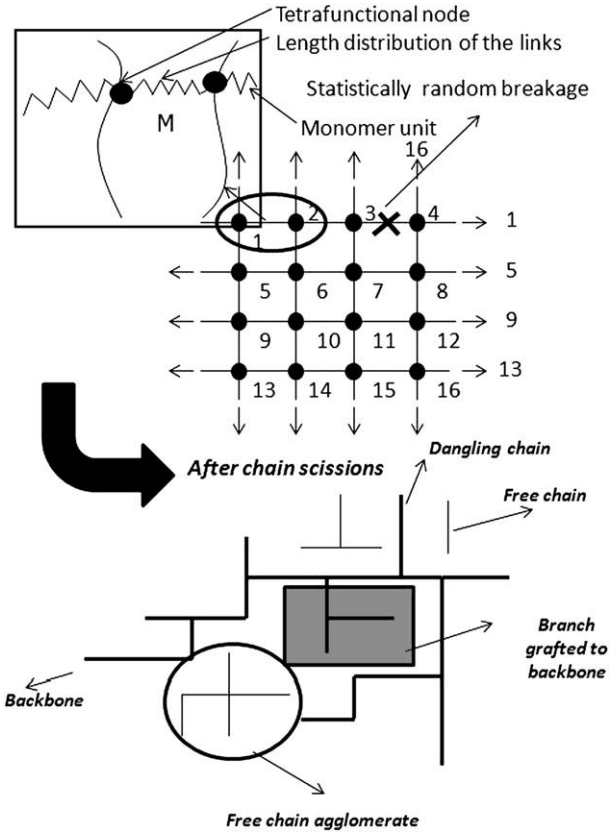

Fig. 11. Scheme of model network.

linked to each other by a bifunctional node. In other words, the dangling chains linked to this node are ignored in the calculation of the average molar mass of the active network.

The model parameters are the number of nodes, the molar distribution of the links (i.e. the distribution of their number of units), and the number of scissions. Calculations were performed with 4900 nodes (9800 links). In order to check and improve the statistic, six simulations were performed and the results presented are the average of these. Moreover, it has been checked that the use of only 625 nodes gives the same mean estimations, but with a larger standard deviation.

The presented model does not include any crosslinking process. The latter can be considered by increasing the initial crosslink density of the network submitted to the degradation kinetic. As shown previously, E-CR degradation primarily consists of chain scissions, except during the first stage of degradation, where slight crosslinking occurs. Therefore, one can consider the degradation kinetic of this material as the chain scission process of an E-CR initially slightly more crosslinked than the real initial material. From the previous extrapolation at 0 kGy of the modulus (cf. Fig. 3), we consider an initial average chain length between crosslinks N_c of 66 units. So this model accounts for a total of 646,800 units (66×9800).

Additionally, the calculation needs the knowledge of the distribution of the number of units between crosslinks in the initial material. The crosslinking process is initiated by peroxide. The latter is assumed to be randomly distributed in the uncrosslinked EPDM. This means that the crosslinking can be assumed to occur between chains with the conformational state following the Gaussian statistic. Thus, the probability $P(r)$ for the distance between two crosslinks having a distance r will obey:

$$P(r) = \frac{4\pi r^2}{2/3\pi\langle r^2\rangle^{3/2}} \exp\left(\frac{-3r^2}{2\langle r^2\rangle}\right) \tag{17}$$

with $\sqrt{\langle r^2\rangle}$ being the average distance between two crosslinks given by:

$$\left\langle r^2\right\rangle = C_{\mathrm{EPDM}} N_c b^2 \tag{18}$$

where C_{EPDM} ($C_{\mathrm{EPDM}} = 6.4$) is the EPDM characteristic ratio, which in turn is an average value of the characteristic ratio of the polyethylene and the polypropylene ($C_{\mathrm{PE}} = 6.8$ and $C_{\mathrm{PP}} = 5.5$ [31]). b is the length of the monomer unit of EPDM, which in this case is the same as polyethylene: $b = 0.308$ nm. In our case, R_c is determined to be 13 nm.

Fig. 12 presents the calculated evolution of the total sol fraction, and of the sol fraction made of chains containing at least two nodes and considered to be "free chain agglomerates", versus the number of scissions per the initial total number of units N_s. As we expected, the calculation indicates that the sol fraction at the beginning of the degradation process is mainly comprised of chain portions coming from dangling chains. As the number of scissions increases, free chain agglomerates rapidly become significant in the sol fraction: for 20% of soluble fraction, 9.2% is comprised of free chain agglomerates.

The calculations also predict the molar mass, and the number of free chain agglomerates and branches (belonging to the backbone) (cf. Fig. 13) [24]. The scissions lead to a rapid increase in the number of branches followed by a stabilization for a number of chain scissions per unit around 10^{-2}. At this level of damage, a large number of branches become separated from the network backbone and end up as free chain agglomerates. However, both types of agglomerates show an increase in size.

N_s obtained from simulation at a given sol fraction can be compared to the experimental results from the same sol fraction

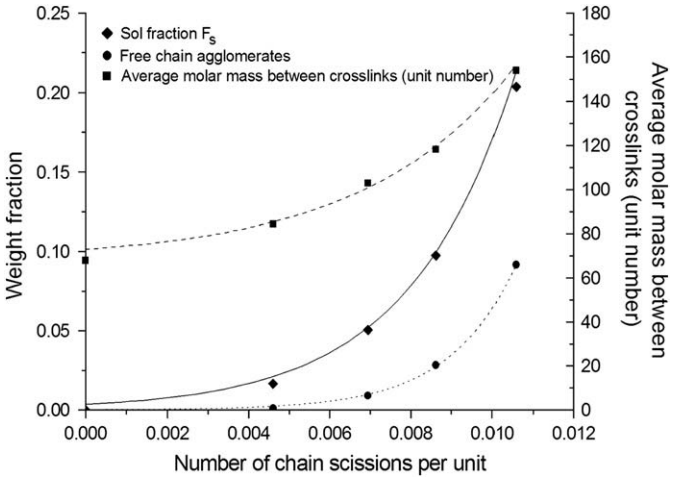

Fig. 12. Calculated total sol fraction, free chain agglomerate fraction and average molar mass between crosslinks as a function of the number chain scissions per unit (calculation performed with an initial average length of active chains of 66 units).

required to extract an equivalent radiation dose. Fig. 5 shows a non-linear relationship at the beginning of the crosslinking process. Conversely, a linear relationship is evidenced above 50 kGy. The deduced slope, equal to 1.2×10^{-8} scission per unit per gray enables us to estimate a chain scission yield. It is found that a $G_{\text{s-sim}}$ equals 3.9×10^{-7} mol/J. This value is very close to that deduced from the Charlesby's model. Thus, this numerical model is roughly equivalent to the Charlesby's one for radiation doses above 50 kGy. The very high scission value needed at the beginning of the simulated degradation process in order to obtain the correct sol fraction value is due to the fact that the initial simulated network does not contain any dangling chains, in contrast to Charlesby's approach, which implicitly assumes their presence. Thus, the formation of sol fraction from such a network needs first the scission of chains, prior to the formation of soluble chains arising from the created dangling chains. Once such a process has been taken into account by a large initial scission kinetic, it can be considered, for sufficiently high dose (above 50 kGy), that the network characteristics simulated by our approach are roughly similar to those of the network modeled by Charlesby's approach.

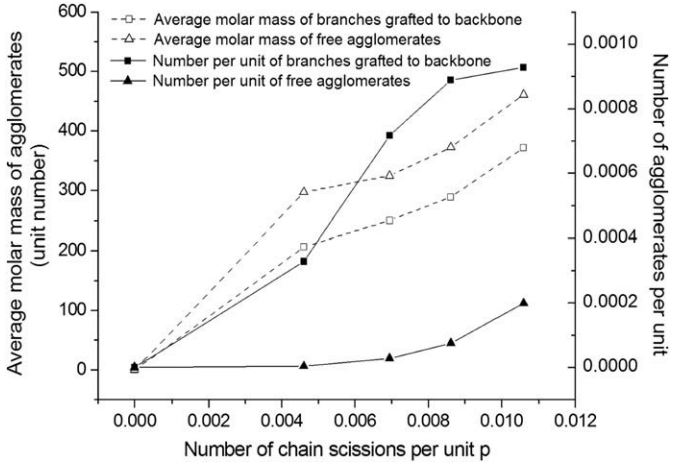

Fig. 13. Size and number per unit of the free agglomerates and of branches grafted to backbone as a function of the number of chain scission per unit.

From the calculated average molar mass L_{av} (expressed in unit number) of the network "backbone", an average network density can be deduced, and ultimately the modulus of the calculated network (using the relation (12)) [24]:

$$G_{sim} = \frac{\rho RT(F_{Backbone})^{1/3}}{wL_{av}} \quad (19)$$

$F_{Backbone}$ is the fraction of active chains in the gel. This means that we assume here that the dangling chains of the backbone are considered to form part of the soluble chains.

Fig. 2 presents the modulus G_{sim} deduced from the simulation as a function of the radiation dose. As seen on the same figure, the simulated results correctly reproduce the modulus decrease. Note that there is an underestimation of around 20% between the calculated result and the experimental data in the dose range [50–400 kGy]. This can be easily explained by the uncertainty in the initial crosslink density of the material. Actually, this value is probably underestimated since it is calculated with the assumption of the absence of dangling chains; the real material necessarily contains these dangling chains. Whatever the radiation dose, making the assumption that the material at doses greater than or equal to 50 kGy is correctly simulated, the calculation indicates that around 20% of the gel is comprised of dangling chains. It is reasonable to consider that their content in the non-irradiated material is of the same order. As discussed in several studies [10,31,32], the presence of dangling chains in a network results in a reduction of the active chain concentration. Actually their effect is complex: Dusek et al. [33] or Mark et al. [10] have shown that they act as a kind of diluent which is however less mobile than a low-molar weight compound or sol. Therefore, the crosslink density, and thus the average number of units in between crosslinks of non-irradiated material used in the calculation (deduced from the modulus extrapolation at 0 kGy with an assumption of 0% sol fraction) is likely underestimated by 10–20%. Such a correction would lead to a very good model of the modulus evolution of E-CR.

Fig. 14 shows the simulation of the distribution of the molar mass between active crosslinks in the E-CR degraded network for the different radiation doses. As expected, chain scissions lead to the appearance of supplementary peaks centered on values equal to multiples of the initial average length of the chain in the E-CR network. Thus this simplified model correctly accounts for the trends observed in thermoporosimetry: an increase in the average molar mass between crosslinks of the network, an increase in their distribution width towards the larger length, and the appearance of a modulation of the distribution.

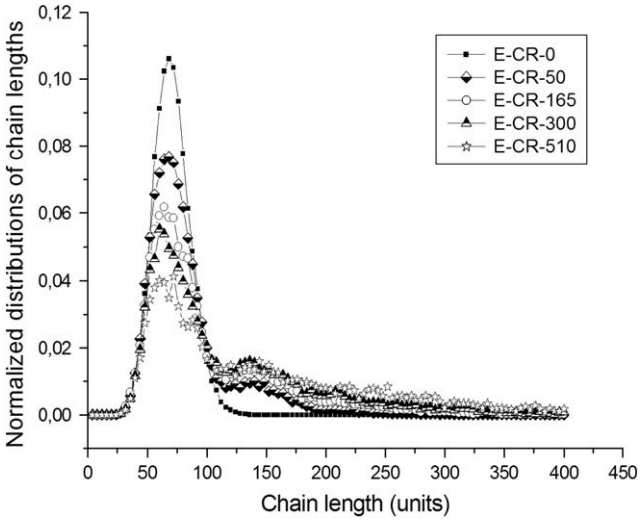

Fig. 14. Normalized distribution of chain lengths calculated for E-CR as a function of irradiation dose (for a volume of 689,000 units, results are average of six calculation runs).

4. Discussion

The decrease in the average crosslink density should increase the strain at break of the E-CR. This is experimentally observed in the case of less crosslinked E-CR2 min and E-CR3 min. Indeed, compared to virgin E-CR, these samples have a larger strain at break correlated to their average crosslink density deduced from modulus measurements. Conversely, for irradiated E-CR, the average crosslink density decreases while the strain and stress at break decrease. Therefore the average crosslink density is not the only pertinent parameter required to predict rupture behavior: One must also consider the architecture of the network. The decrease in homogeneity of the network can be evaluated from the experimental results of thermoporosimetry, which are qualitatively in agreement with the calculated distribution of the average molar mass between active nodes. However it is noteworthy that E-CR3 min and E-CR-300 have similar elastic modulus at 80 °C and the same results in thermoporosimetry (i.e. a similar distribution of elastic network heterogeneity), whereas their rupture behavior is very different. The main difference between these materials is the sol fraction. The calculations have shown that this sol fraction contains more and more free chain agglomerates as radiation dose increases. Simultaneously, degradation leads to creation of larger and larger branches grafted to the network backbone. Thus the network architecture becomes very irregular. This means that the network contains an increasing number of weakened zones, which can lead to crack initiation. This phenomenon is concomitant with an increase in the average length of the active chains of the network. However, given the distributed character of these chain lengths, the elongation at break is likely controlled by the shortest chains, percolating through the whole sample. Thermoporosimetry and calculations clearly show the modification of the initial distribution into a multimodal one, in which the fundamental mode corresponds to the initial population. At the start of the degradation process, this population controls the elongation at break, while obviously at elevated radiation doses, the memory of this population vanishes while longer populations lead to an increase in elongation at break. By appreciating these mechanisms, one can propose an underlying cause for the rupture behavior of all the samples.

The elongation and stress at break of E-CR first decrease with radiation doses, because of the more numerous weak crosslinks in the network. Up to 300 kGy, this effect is insufficiently counterbalanced by the increase in the average chain length in the network, since the network is still mainly constituted of the initial population of chains. On the other hand, the slight increase in the strain at break observed in the case of the most irradiated sample (E-CR-510) might be due to the degradation being severe enough to completely destroy the "percolation" of these initial chains.

In the case of E-NC, the evolution of the rupture behavior with radiation dose is the result of the concomitant crosslinking and bond-breaking processes. Unfortunately, the same simulation approach cannot be similarly applied to E-NC due to the important crosslinking process occurring in the same time as the chain scission one. However, the irradiated materials can be envisioned as an initial network whose stress and strain at break are controlled by an initial average length, one which decreases with the radiation dose, submitted to a degradation process which creates large free agglomerates. Thus, the E-NC-50 is a loose network, with an

expected large strain at break, but with a large sol fraction, having numerous weakened zones, which decrease the strain at break. Then further irradiation leads to more crosslinks in the initial network, which would be expected to decrease the strain at break, although kept in check by the chain scissions. Thus, at higher doses, the irradiated material can be seen as an initially crosslinked network with an average mass between crosslinks larger than that of the E-CR-0 network. This should lead to a strain at break much larger than that of this material. But the presence of sol fraction, i.e. of weakened links, leads to a decrease in strain at break to a smaller value, which is still above E-NC-510.

5. Conclusions

Different EPDM elastomers with different crosslink densities were processed in order to evaluate the influence of gamma irradiation on their properties. Depending on the initial crosslink density of sample, irradiation can lead to supplementary crosslinking of polymer chains. This mechanism is important for initial unlinked sample. For samples with initial high crosslink density, this mechanism also occurs at the lowest radiation doses and becomes negligible at high doses, where chain scissions mainly occur. These different phenomena are correctly accounted for by the Charlesby–Pinner modeling approach for doses equal or above 50 kGy. This model indicates that, within the experimental conditions of our study, the chain scission mechanism involved in the degradation of the crosslinked EPDM is proportional to the radiation dose. In the case of the initially uncrosslinked EDPM, the experimental results at high radiation doses suggest that the scission mechanism follows the same kinetic, i.e. a proportionality between scission and radiation dose. Assuming such a scission kinetic, a crosslinking kinetic can be estimated, and is found to be not proportional to the radiation dose. This mechanism saturates when the crosslinking density is close to that estimated for non-irradiated crosslinked EPDM. This suggests that the crosslinking mechanism induced either by irradiation or by chemical (peroxide) curing should be very similar.

Concerning the initially crosslinked material, the consequences of the chain scissions are a decrease in the elastic modulus, and also in the strain at break. This behavior is opposite to that expected for materials with increasing average chain length between crosslinks. This surprising phenomenon is attributed to the presence of defects in network. Thermoporosimetry measurements were performed to characterize these defects, in particular the distribution of the average molar mass between crosslinks. They show an increase in the distribution towards longer chains with increasing radiation dose, and for the highest radiation doses studied, a multimodal distribution. However, the experimental distributions found in the case of virgin networks with low crosslink density are much larger than that obtained with the most irradiated material, whereas their strains at break are more elevated than that observed for the aged sample. Thus it seems that the type of heterogeneity evidenced by such measurement cannot fully explain the evolution of the rupture behavior under ageing.

To produce new insights, a model has been developed enabling simulation of the chain scission mechanism of an elastomer network. It successfully enables prediction of the evolution of the elastic modulus of the material, based on an estimation of average chain length between active crosslinks. The appearance, at high irradiation dose, of the multimodality of distribution of the molar mass between crosslink is also predicted. This model furthermore predicts the proportion of free chains, of free chain agglomerates and of branches linked to the network backbone. From this information on the evolution of the network architecture, two key parameters have been identified for the rupture behavior and its evolution with ageing. The first is the average molar mass between crosslinks, which controls the rupture of a network in the absence of defects. The second is the proportion of weakened zones comprised of large free agglomerates, and large branched chains in the mechanically active network backbone, which degrade the rupture property.

Acknowledgements

It is a pleasure to acknowledge the joint research program "COPOLA" between EDF, NEXANS France, LABORELEC, CEA, INRA and CNRS. The authors also thank J.C. Majeste for GPC analyses, Cedric Lorthioir for helpful discussions and Julian de Marchi for corrections of English.

References

[1] Rivaton A, Cambon S, Gardette JL. Nuclear Instruments and Methods in Physics Research B 2005;227:343–56.
[2] Rivaton A, Cambon S, Gardette JL. Nuclear Instruments and Methods in Physics Research B 2005;227:357–68.
[3] Celette N, Stevenson I, Davenas J, David L, Vigier G. Nuclear Instruments and Methods in Physics Research B 2001;185:305–10.
[4] Celette N, Stevenson I, David L, Vigier G, Seytre G. Polymer International 2004;53:495–505.
[5] Assink RA, Gillen KT, Sanderson B. Polymer 2002;43:1349–55.
[6] Celina M, Gillen KT, Wise J, Clough RL. Radiation Physics and Chemistry 1996;48:613–26.
[7] Assink RA, Celina M, Gillen KT, Clough RL, Alam TM. Polymer Degradation and Stability 2001;73:355–62.
[8] Bateja SK. Journal of Applied Polymer Science 1983;28:861–72.
[9] Planes E, Chazeau L, Vigier G, Chenal JM, Stuhldreier T. Journal of Polymer Science, Part B: Polymer Physics, submitted for publication.
[10] Andrady AL, Llorente MA, Sharaf MA, Rahalkar RR, Mark JE. Journal of Applied Polymer Science 1981;26:1829–36.
[11] Mark JE, Tang MY. Journal of Polymer Science: Polymer Physics Edition 1984;22:1849–55.
[12] Llorente MA, Andrady AL, Mark JE. Journal of Polymer Science 1981;19: 621–30.
[13] Madkour T, Mark JE. Polymer Bulletin 1993;31:615–21.
[14] Termonia Y. Macromolecules 1989;22:3633–8.
[15] Termonia Y. Macromolecules 1990;23:1481–3.
[16] Grest GS, Kremer K. Macromolecules 1990;23:4994–5000.
[17] Charlesby A, Pinner SH. Proceedings of the Royal Society of London 1959;A249:367–86.
[18] Charlesby A. Proceedings of the Royal Society of London 1954;A222:542–57.
[19] Rottach DR, Curro JG, Grest GS, Thompson AP. Macromolecules 2004;37: 5468–73.
[20] Rottach DR, Curro JG, Budzien J, Grest GS, Svaneborg C, Everaers R. Macromolecules 2006;39:5521–30.
[21] Rottach DR, Curro JG, Budzien J, Grest GS, Svaneborg C, Everaers R. Macromolecules 2007;40:131–9.
[22] Vallat MF, Ruch F, David MO. European Polymer Journal 2004;40:1575–86.
[23] Orza RA, Magusin PCMM, Litvinov VM, van Duin M, Michels MAJ. Macromolecules 2007;40:8999–9008.
[24] Flory PJ, Rehner J. Journal of Chemical Physics 1943;11:521–6.
[25] Valentin JL, Carreto-Gonzalez J, Mora-Barrantes I, Chasse W, Saalwachter K. Macromolecules 2007;11:4717–29.
[26] Honiball D, Huson MG, McGill WJ. Journal of Polymer Science, Part B: Polymer Physics 1988;26:2413–31.
[27] Qin Q, McKenna GB. Journal of Polymer Science, Part B: Polymer Physics 2006;44:3475–86.
[28] Khelidj N, Colin X, Audouin L, Verdu J, Monchy-Leroy C, Prunier V. Polymer Degradation and Stability 2006;91(7):1593–7.
[29] Decker C, Mayo FR, Richardson H. Journal of Polymer Science: Polymer Chemistry Edition 1973;11:2879–98.
[30] Colin X, Richaud E, Verdu J, Monchy-Leroy C. Conference IRAP 2008, Kinetic modelling of radiochemical ageing of ethylene–propylene copolymers, conf. proceeding.
[31] Sperling LH. Introduction to physical polymer science. 2nd ed. Wiley Interscience; 1992.
[32] Villar MA, Valles EM. Macromolecules 1996;29:4081–9.
[33] Dusek K, Duskova-Smrckova M, Fedderly JJ, Lee GF, Lee JD, Hartmann B. Macromolecular Chemistry and Physics 2002;203:1936–48.